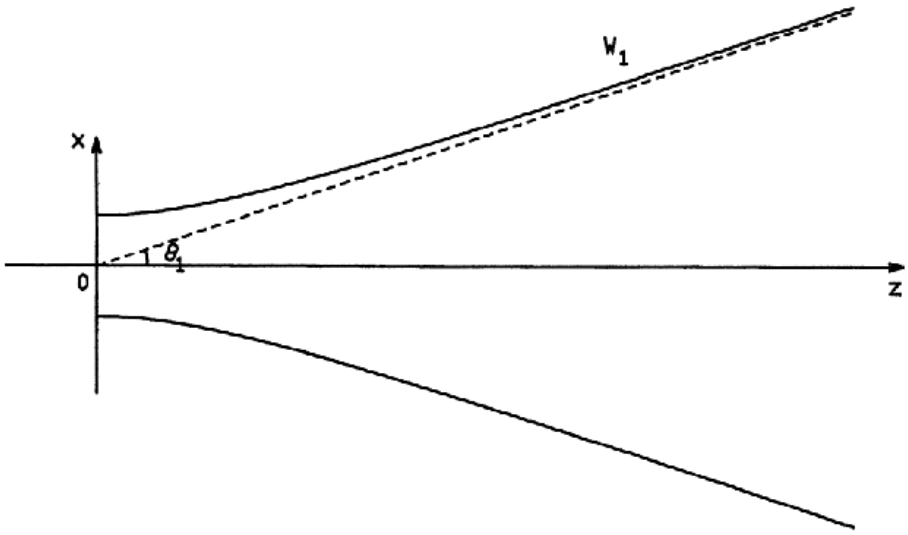

Figure 2.19 Variation of the spot size along x-axis direction, $W_1(z)$.

index $n_1 = 3.5$, cladding index $n_0 = 3.17$, and core width and thickness of $2a = 1.5\,\mu\text{m}$ and $2d = 0.15\,\mu\text{m}$, respectively. The electric field distribution of the waveguide is calculated by using the finite element method waveguide analysis, which will be described in Chapter 6, and is Gaussian fitted to obtain the spot sizes w_1 and w_2 along x- and y-axis directions. Gaussian-fitted spot sizes w_1 and w_2 are

$$\begin{cases} w_1 = 0.88\,\mu\text{m} \\ w_2 = 0.35\,\mu\text{m}. \end{cases} \tag{2.112}$$

The divergence angles θ_1 and θ_2 are then obtained, by Eqs. (2.111b) and (2.112) as

$$\begin{cases} \theta_1 = 0.51\ (\text{rad.}) = 29.4\ (\text{degree}) \\ \theta_2 = 0.95\ (\text{rad.}) = 54.4\ (\text{degree}). \end{cases} \tag{2.113}$$

It is known from the above result that the radiation field from the semiconductor laser diode has an elliptic shape and the divergence angle along the thin active-layer (y-axis direction) is much larger than that along the wide active-layer direction (x-axis direction).

2.4. MULTIMODE INTERFERENCE (MMI) DEVICE

Multimode interference devices, based on self-imaging effect [11,12], are very important integrated optical components which can perform many different splitting and combining functions [13–16]. Figure 2.20 shows a schematic

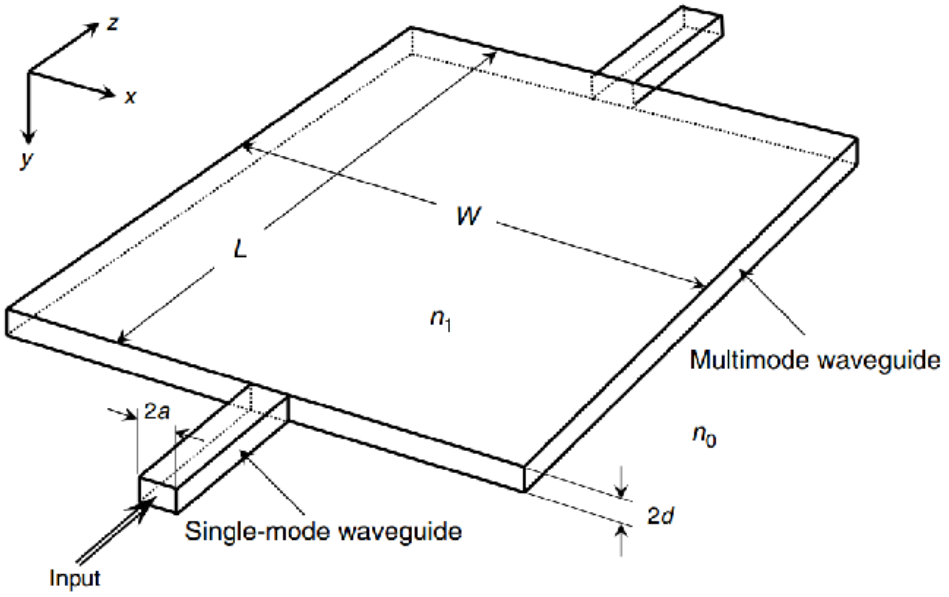

Figure 2.20 Schematic configuration of multimode interference (MMI) waveguide.

configuration of MMI waveguide. The key structure of an MMI device is a waveguide designed to support a large number of modes. The width, thickness and length of the multimode region are W, $2d$ and L, respectively. Single-mode waveguide with core width $2a$ and thickness $2d$ is connected to the multimode waveguide. Refractive indices of the core of single-mode and multimode waveguides are equal to n_1 and the refractive index of the cladding is n_0. Three-dimensional waveguide structure can be reduced to a two-dimensional problem by using an effective index method. The effective index n_{eff} of the core is calculated by solving the eigen-mode equation along y-axis. Figure 2.21 shows two-dimensional configuration of an MMI waveguide of core effective index n_{eff} and cladding refractive index n_0. Electric field in the multimode waveguide is calculated by using Eqs. (2.7)–(2.15). Here waveguide parameters n_1, a and n_s in Eqs. (2.7)–(2.15) are replaced by n_{eff}, $W/2$ and n_0, respectively. Then electric field profile for TE_m mode in the multimode waveguide is expressed by

$$E_y^m(x,y) = \begin{cases} A_m \cos\left(u_m + \dfrac{m\pi}{2}\right) \exp\left[\dfrac{2w_m}{W}\left(x + \dfrac{W}{2}\right) - j\beta_m z\right] & \left(x < -\dfrac{W}{2}\right) \\ A_m \cos\left(\dfrac{2u_m}{W}x - \dfrac{m\pi}{2}\right) \exp(-j\beta_m z) & \left(|x| \leqslant \dfrac{W}{2}\right) \\ A_m \cos\left(u_m - \dfrac{m\pi}{2}\right) \exp\left[-\dfrac{2w_m}{W}\left(x - \dfrac{W}{2}\right) - j\beta_m z\right] & \left(x > \dfrac{W}{2}\right), \end{cases} \tag{2.114}$$

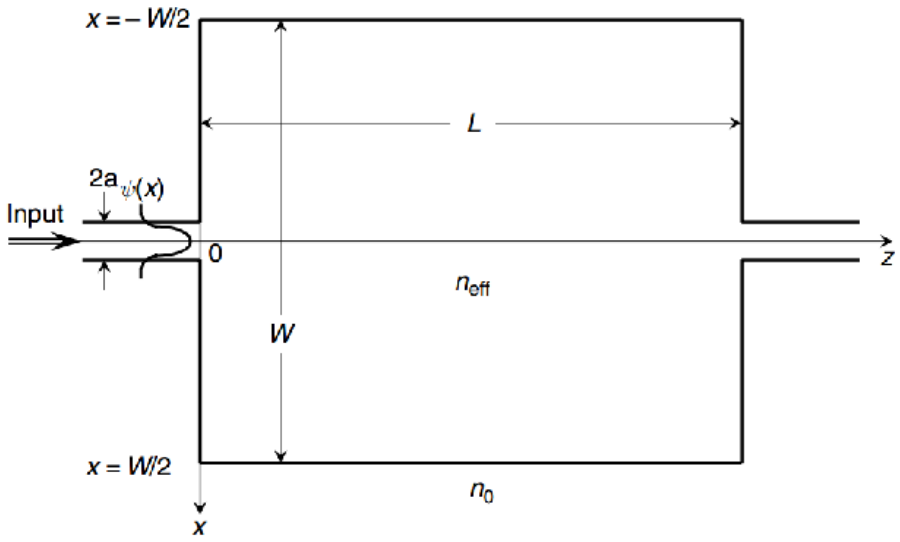

Figure 2.21 Two-dimensional representation of an MMI waveguide.

where u_m and w_m denote the transverse wavenumbers of the m-th mode in the core and cladding and A_m is constant. Transverse wavenumbers are obtained from the eigenvalue equation as

$$w_m = u_m \tan\left(u_m - \frac{m\pi}{2}\right) \tag{2.115}$$

and

$$u_m^2 + w_m^2 = k^2\left(\frac{W}{2}\right)^2 (n_{\text{eff}}^2 - n_0^2) \equiv v^2. \tag{2.116}$$

When the core width W of MMI region is large, the normalized frequency v also becomes large. It is known from Fig. 2.3 that when v becomes large, u_m approaches $u_m \cong (m+1)\,\pi/2$. Then the propagation constant β_m is approximately expressed as

$$\beta_m = \sqrt{k^2 n_{\text{eff}}^2 - (2u_m/W)^2} \cong kn_{\text{eff}} - \frac{(m+1)^2\lambda}{4n_{\text{eff}}W^2}\pi. \tag{2.117}$$

The total electric field in the MMI region is obtained by

$$\Psi(x,z) = \sum_{m=0}^{M} E_y^m(x,z) = e^{-jkn_{\text{eff}}z} \sum_{m=0}^{M} A_m \cos\left[\frac{(m+1)\pi}{W}x - \frac{m\pi}{2}\right] \times \exp\left[j\frac{(m+1)^2\pi\lambda}{4n_{\text{eff}}W^2}z\right], \tag{2.118}$$

where M denotes the maximum mode number. At $z=0$, $\Psi(x,0)$ coincides with the electric field of the input waveguide $\psi(x)$. Then the electric field amplitude A_m is obtained from Eq. (2.118) as

$$A_m = \frac{2}{W}\int_{-W/2}^{W/2} \psi(x)\cos\left[\frac{(m+1)\pi}{W}x - \frac{m\pi}{2}\right]dx. \tag{2.119}$$

For simplicity, we consider the case in which the input single-mode waveguide is connected to the center of the multimode waveguide. In this condition, modes in MMI region become only symmetrical modes; that is, m becomes an even number $m=2\ell$ (ℓ : integer). At the point $z=n_{\text{eff}}W^2/\lambda$, the phase term in Eq. (2.118) reduces to

$$\exp\left[j\frac{(m+1)^2\pi\lambda}{4n_{\text{eff}}W^2}z\right] = \exp\left[j\ell(\ell+1)\pi + j\frac{\pi}{4}\right] = \exp\left(j\frac{\pi}{4}\right). \tag{2.120}$$

We now define the characteristic length L_{MMI} as

$$L_{\text{MMI}} = \frac{n_{\text{eff}}W^2}{\lambda}. \tag{2.121}$$

The electric field profile at the MMI length L_{MMI} is then obtained from Eq. (2.118) as

$$\Psi(x, L_{\text{MMI}}) = e^{-jkn_{\text{eff}}L_{\text{MMI}}+j\pi/4}\sum_{m=0}^{M} A_m \cos\left[\frac{(m+1)\pi}{W}x - \frac{m\pi}{2}\right]. \tag{2.122}$$

Since $\Psi(x,0)$ in Eq. (2.118) is the electric field of the input waveguide $\psi(x)$, the above equation is rewritten as

$$\Psi(x, L_{\text{MMI}}) = \psi(x)e^{-jkn_{\text{eff}}L_{\text{MMI}}+j\pi/4}. \tag{2.123}$$

It is confirmed that the input electric field $\psi(x)$ is reproduced at the specific length L_{MMI} with slight phase retardation. Self-imaging characteristics in MMI waveguide are confirmed by the Beam Propagation Method (BPM) simulation. Figure 2.22 shows the image formation for light input at the center of MMI waveguide. Refractive-index difference of the waveguide is $\Delta = 0.75\%$ and the wavelength of light is $\lambda = 1.55\,\mu\text{m}$. Waveguide parameters of the single-mode input waveguide are $2a = 7\,\mu\text{m}$ and $2d = 6\,\mu\text{m}$ and those of MMI are $W = 150\,\mu\text{m}$ and $L = 25.99\,\text{mm}$. Specific length L_{MMI} that is given by Eq. (2.121) is 25.89 mm. Since there is a Goos-Hanshen effect, light field slightly penetrates into cladding region. Therefore, slight correction is necessary for either width W or length L of the MMI region. In Fig. 2.22, correction length of $\delta_L = 100\,\mu\text{m}$ is

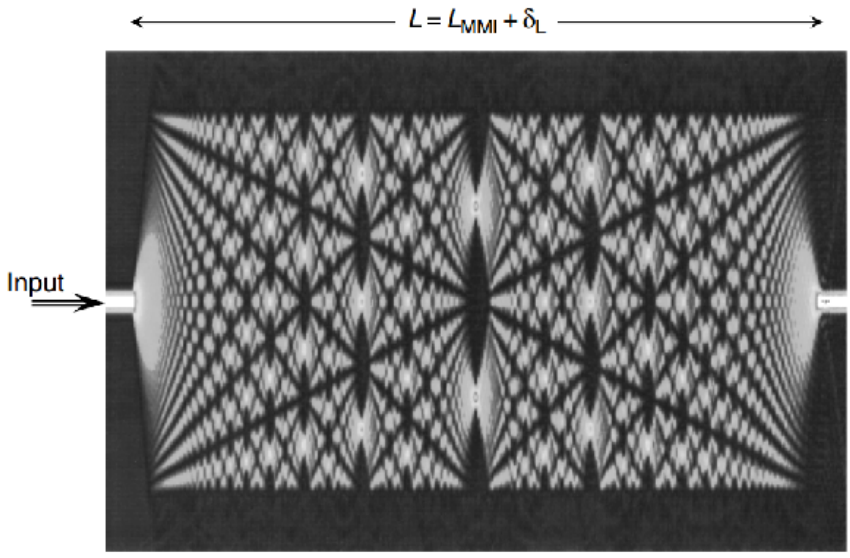

Figure 2.22 Image formation for light input at the center of MMI waveguide.

added to the analytical self-imaging length L_{MMI}. It is known from Fig. 2.22 that N images are formed at $z = L_{MMI}/N$, for any integer N. Figure 2.23 shows light-splitting characteristics of MMI waveguide with a length of $L_{MMI}/8 + \delta'_L$, where $\delta'_L = 105\,\mu m$. Output waveguides are located at $x_i = (4.5 - i)\,W/8$ for i-th ($i = 1, 2, \ldots, 8$) waveguide. Figure 2.24 shows theoretical and experimental splitting characteristics of 1×8 MMI splitter at $\lambda = 1.55\,\mu m$. MMI splitter is made of silica waveguide with $2a = 7\,\mu m$, $2d = 6\,\mu m$ and $\Delta = 0.75\%$. Splitting

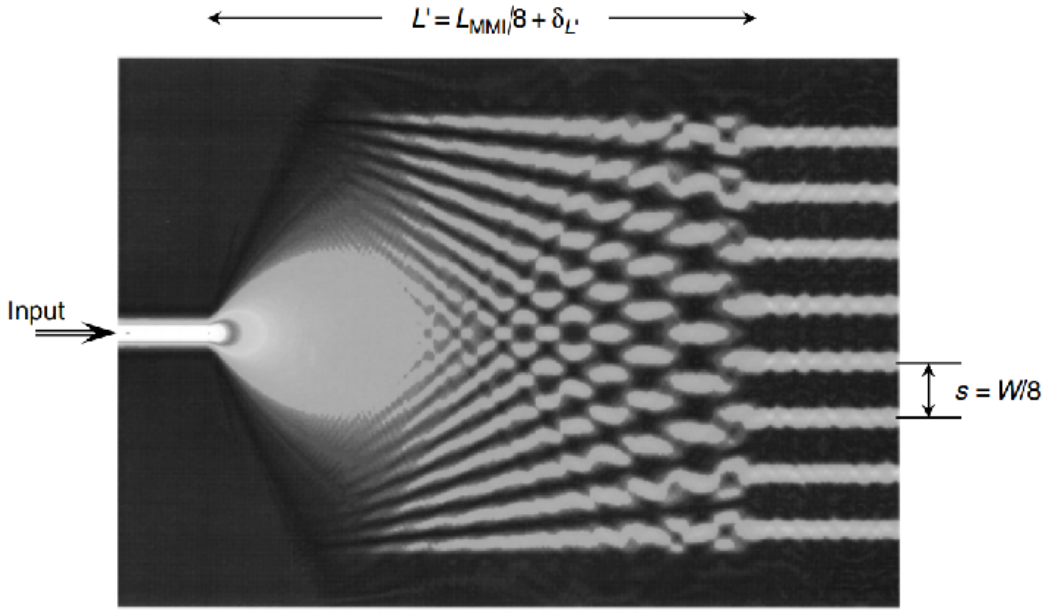

Figure 2.23 Light-splitting characteristics of MMI waveguide with a length of LMMI/8.

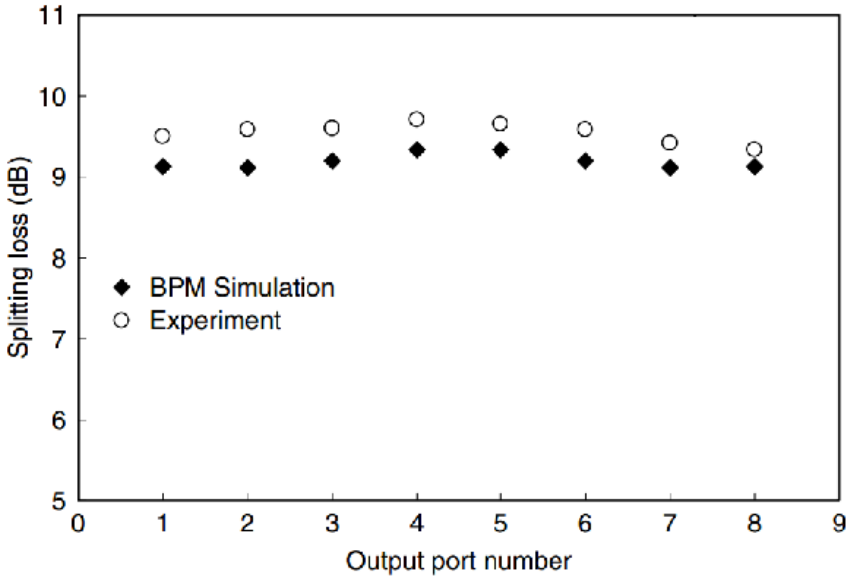

Figure 2.24 Theoretical and experimental splitting characteristics of 1×8 MMI splitter.

loss of 1/8 corresponds to 9 dB. Therefore, it is known that the excess loss of each output port is less than 1 dB.

When an input waveguide is placed at the proper position from the center of MMI waveguide, two-fold images are formed with equal amplitude at the distance of [17]

$$L_{3\,\mathrm{dB}} = \frac{2}{3} \cdot \frac{n_{\mathrm{eff}} W^2}{\lambda}, \tag{2.124a}$$

$$W = (N+1)s \qquad (N=2), \tag{2.124b}$$

where s denotes the separation of output waveguides. Figure 2.25 shows a 3-dB coupler based on the 2×2 MMI splitter. BPM simulation is required in order to accurately determine the 3-dB coupler configuration. Light propagation characteristics in the MMI 3-dB coupler are shown in Fig. 2.26. The length of 3-dB coupler is determined to be $L = L_{3\,\mathrm{dB}} + \delta_{3\,\mathrm{dB}} (\delta_{3\,\mathrm{dB}} = 200\,\mu\mathrm{m})$ by the BPM

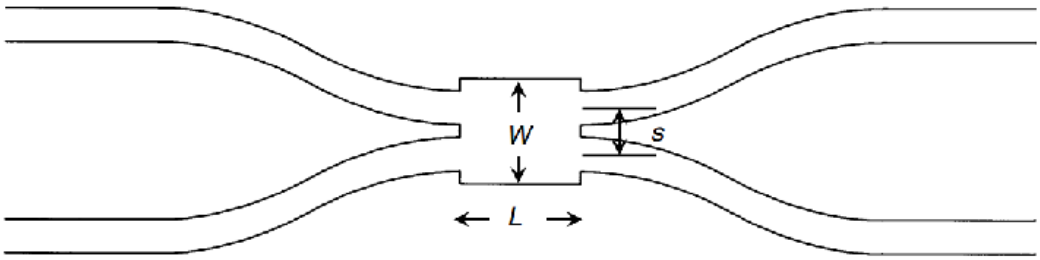

Figure 2.25 3-dB coupler based on the 2×2 MMI splitter.

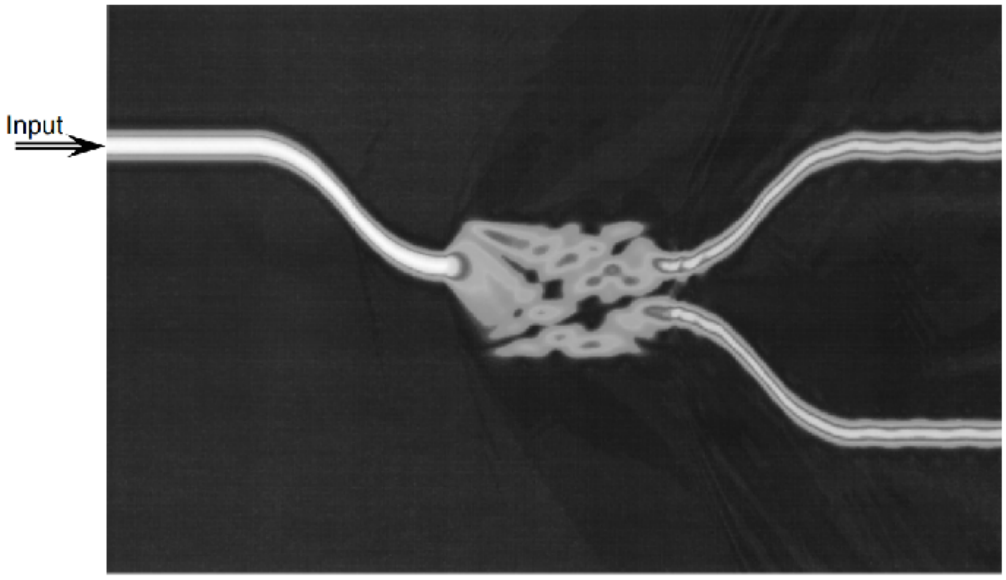

Figure 2.26 Light propagation characteristics of MMI 3-dB coupler.

calculation. Figure 2.27 shows spectral splitting ratios of MMI 3-dB coupler and codirectional coupler (see Section 4.2) and spectral insertion loss of MMI 3-dB coupler. It is known from the figure that coupling ratio of MMI 3-dB coupler is almost insensitive to wavelength as compared to codirectional coupler. This is a great advantage of MMI 3-dB coupler over a codirectional coupler. However,

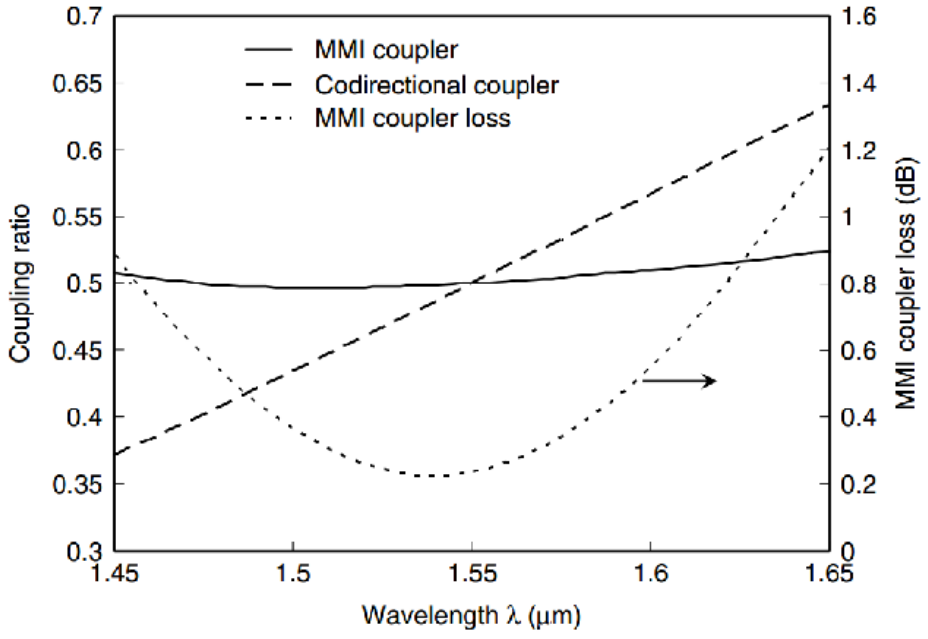

Figure 2.27 Spectral splitting ratios of MMI 3-dB coupler and codirectional coupler and spectral insertion loss of MMI 3-dB coupler.

we should take notice of two facts. First, insertion loss of MMI is not zero even in theoretical simulation. Theoretical insertion loss of the MMI 3-dB coupler is about 0.22 dB at the minimum. Second, the insertion loss of MMI coupler rapidly increases as wavelength departs from the optimal wavelength.

When phase of the input light is properly adjusted $1 \times N$ MMI splitter functions as $N \times 1$ combiner. Figure 2.28 shows light propagation characteristics in MMI 16×1 combiner. Complex electric field g_i in the i-th input waveguide is

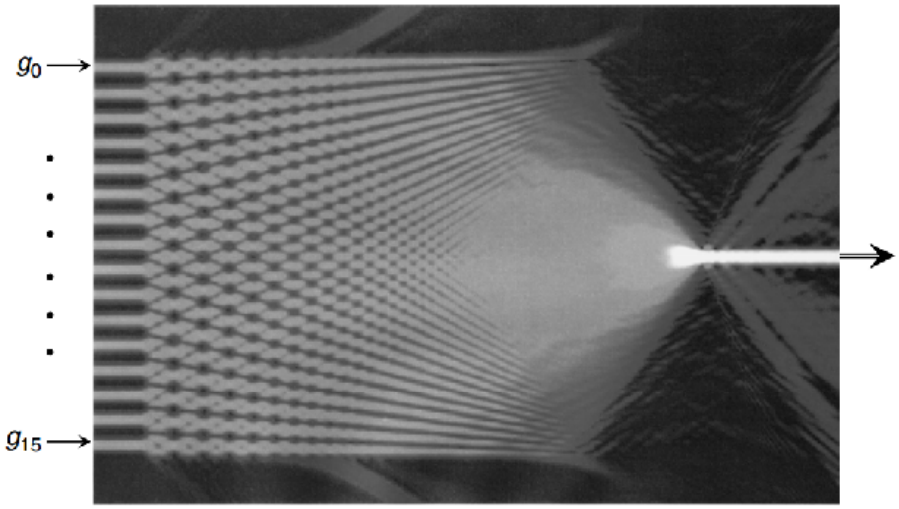

(a)

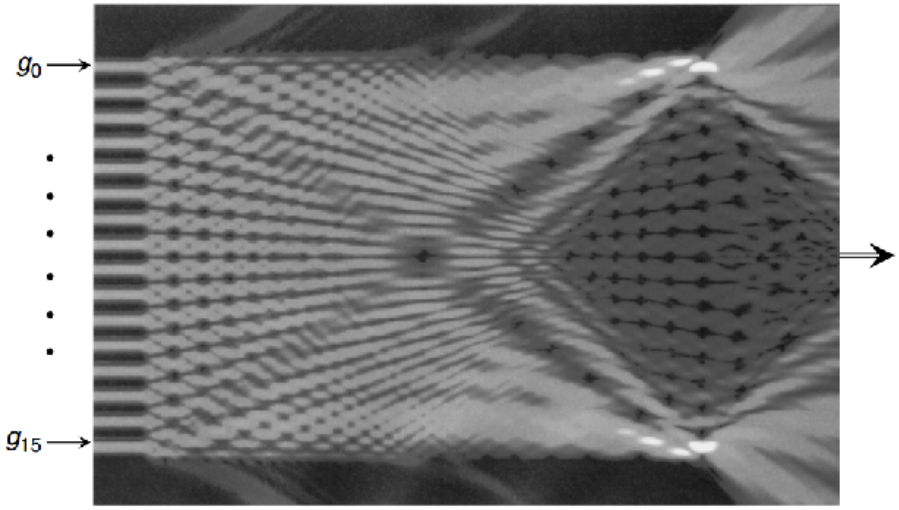

(b)

Figure 2.28 Light propagation characteristics in MMI 16×1 combiner: (a) Amplitudes of g_i's are equal and their phases are properly adjusted; and (b) amplitudes of g_i's are equal and their phases are completely out of phase.

given by $g_i = a_i \exp(j\theta_i)$, where a_i and θ_i denote amplitude and phase of g_i. In the BPM simulation shown in Fig. 2.28a, amplitudes of g_i's are set to be equal and their phases are properly adjusted. Every light beam from 16 input ports constructively interfere to form a single output image at the distance of $L = L_{\mathrm{MMI}}/16 + \delta_{\mathrm{I}}$, where $\delta_{\mathrm{I}} = 140\,\mu\mathrm{m}$. It is shown by a number of numerical simulations that MMI $N \times 1$ combiner has a unique property in which we can obtain coherent summation of the input electric field as

$$T = \left| \frac{1}{N} \sum_{i=0}^{N-1} g_i \right|^2 = \left| \frac{1}{N} \sum_{i=0}^{N-1} a_i e^{j\theta_i} \right|^2 . \tag{2.125}$$

Numerical simulation was confirmed by the experiment using 16-tap ($N = 16$) coherent transversal filter [18]. The device was fabricated using silica-based planar lightwave circuits. The core size and refractive-index difference of the waveguides are $7\,\mu\mathrm{m} \times 7\,\mu\mathrm{m}$ and 0.75%, respectively. Figure 2.29 compares the experimental normalized output power with the theoretical one given by Eq. (2.125). Complex electric fields of even and odd ports were set to be $g_i = 1$ ($i = 0, 2, \ldots, 14$) and $g_i = \exp(j\alpha)$ ($i = 1, 3, \ldots, 15$), respectively. Phase shift α was introduced to the waveguide by the thermo-optic effect. The output power of the MMI $N \times 1$ combiner is given from Eq. (2.125) by

$$T(\alpha) = \left| \frac{1}{N}(1 + e^{j\alpha}) \frac{N}{2} \right|^2 = \left| \cos\left(\frac{\alpha}{2}\right) \right|^2 . \tag{2.126}$$

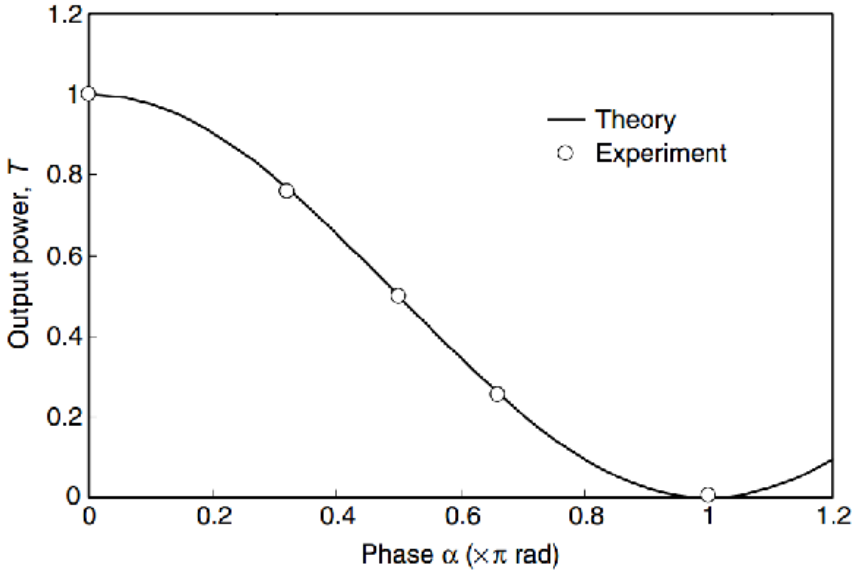

Figure 2.29 Normalized output power T of the 16×1 MMI combiner.

Solid line in Fig. 2.29 shows theoretical curve $|\cos(\alpha/2)|^2$ and circles are experimental values for $\alpha = 0, \pi/3, \pi/2, 2\pi/3$ and π, respectively. It is confirmed that the collective summation of complex electric fields is obtained by using MMI combiner.

REFERENCES

[1] Marcuse, D. 1982. *Light Transmission Optics*. New York: Van Nostrand Reinhold.

[2] Marcuse, D. 1974. *Theory of Optical Waveguides*. New York: Academic Press.

[3] Unger, H. G. 1977. *Planar Optical Waveguides and Fibers*. Oxford: Clarendon Press.

[4] Kressel, H. and J. K. Butler. 1977. *Semiconductor Lasers and Heterojunction LEDs*. New York: Academic Press.

[5] Marcatili, E. A. J. 1969. Dielectric rectangular waveguide and directional coupler for integrated optics. *Bell Syst. Tech. J.* 48:2071–2102.

[6] Kumar, A., K. Thyagarajan and A. K. Ghatak. 1983. Analysis of rectangular-core dielectric waveguides—An accurate perturbation approach. *Opt. Lett.* 8:63–65.

[7] Goell, J. E. 1969. A circular harmonic computer analysis of rectangular dielectric waveguides. *Bell Syst. Tech. J.* 48:2133–2160.

[8] Knox, R. M. and P. P. Toulios. 1970. Integrated circuits for the millimeter through optical frequency range. *Symposium on Submillimeter Waves*, Polytechnic Institute of Brooklyn, pp. 497–516.

[9] Tamir, T. 1975. *Integrated Optics*. Chap. 2, Berlin: Springer-Verlag.

[10] Born, M. and E. Wolf. 1970. *Principles of Optics*. Oxford: Pergamon Press.

[11] Bryngdahl, O. 1973. Image formation using self-imaging techniques. *J. Opt. Soc. Amer.* 63:416–419.

[12] Ulrich, R. 1975. Image formation by phase coincidences in optical waveguides. *Opt. Commun.* 13:259–264.

[13] Niemeier, T. and R. Ulrich. 1986. Quadrature outputs from fiber interferometer with 4×4 coupler. *Opt. Lett.* 11:677–679.

[14] Veerman, F. B., P. J. Schalkwijk, E. C. M. Pennings, M. K. Smit and B. H. Verbeek. 1992. An optical passive 3-dB TMI-coupler with reduced fabrication tolerance sensitivity. *IEEE J. Lightwave Tech.* 10:306–311.

[15] Bachmann, M., P. A. Besse and H. Melchior. 1994. General self-imaging properties in $N \times N$ multimode interference couplers including phase relations. *Appl. Opt.* 33:3905–3911.

[16] Heaton, J. M. and R. M. Jenkins. 1999. General matrix theory of self-imaging in multimode interference (MMI) couplers. *IEEE Photon. Tech. Lett.* 11:212–214.

[17] Soldano, L. B. and E. C. M. Pennings. 1995. Optical multi-mode interference devices based on self-imaging: Principles and applications. *IEEE J. Lightwave Tech.* 13:615–627.

[18] Okamoto, K., H. Yamada and T. Goh. 1999. Fabrication of coherent optical transversal filter consisting of MMI splitter/combiner and thermo-optic amplitude and phase controllers. *Electron. Lett.* 35:1331–1332.